Suppporting Information

30 July, 2012

Ms. ID: ac-2012-01101b

Enrichment of Cations via Bipolar Electrode Focusing

Eoin Sheridan,[1] Dzmitry Hlushkou,[2] Kyle N. Knust,[1] Ulrich Tallarek,[2]* and Richard M. Crooks[1]*

[1]Department of Chemistry and Biochemistry, Center for Electrochemistry, and the Center for Nano- and Molecular Science and Technology, The University of Texas at Austin, 1 University Station, A5300, Austin, Texas 78712-0165, U.S.A.

[2]Department of Chemistry, Philipps-Universität Marburg, Hans-Meerwein-Strasse, 35032 Marburg, Germany.

8 pages

Chemical and Electrochemical Reactions in the Microchannel

For this study, we assume the following chemical reactions take place in the aqueous Tris-HCl buffer.

(S1)

$$H_2O \leftrightarrow OH^- + H^+ \quad \text{(S2)}$$

The chemical reactions modelled for the carbonate buffer are represented by the following equations:

(S3)

(S4)

$$CO_3^{2-} + H^+ \leftrightarrow HCO_3^- \quad \text{(S5)}$$

(S6)

$$H_2O \leftrightarrow OH^- + H^+ \quad \text{(S7)}$$

The rate of each of the above reactions (eqs S1-S7) is represented by two reaction rate constants k_f and k_b, characterizing the rate of the forward and backward reactions, respectively. The values for the reaction rate constants used for computer simulations are given in Table S1. It should be noted that for this study the molar concentration of the water is assumed to be constant (55.5 M). The reaction terms in eq S1 can be represented by differential equations. For example, the reaction term for hydroxide ions (OH^-), describing the rate of change in concentration in the carbonate buffer system due to the chemical reactions, can be written as:

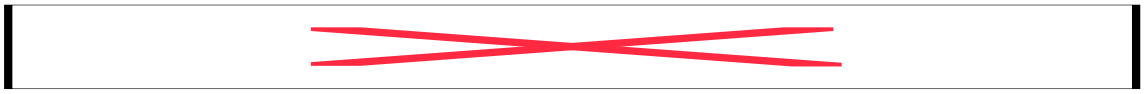

(S8)

Apart from the bulk chemical reactions, the local concentration of species can also change due to electrochemical (faradaic) reactions at the surface of the BPE. For both the Tris-HCl and carbonate buffers, the following anodic and cathodic reactions (eqs S9 and S10, respectively) are assumed to occur:

(S9)

(S10)

The rate of change in the surface activity of the species involved in the faradaic reactions (eqs S9 & S10) can be related to the current density magnitude (j_{BPE}) across the electrode surface as follows:

$$\frac{\partial [H^+]_s}{\partial t} = \frac{j_{BPE}(x)}{10^3 F} \tag{S11}$$

for the anodic pole of the BPE, and:

$$\frac{\partial [OH^-]_s}{\partial t} = \frac{j_{BPE}(x)}{10^3 F} \tag{S12}$$

for the cathodic pole. Here, we assume that the magnitude of the local current density across the BPE surface is not constant. Generally, the local current density can be determined with the Butler-Volmer equation taking into account that the local current

density due to a faradaic reaction depends on the electric potential difference between the floating potential of the BPE and the local potential of the surrounding electrolyte solution. For this study, we employed a simplified approach assuming a linear drop for $j_{BPE}(x)$ from its maxima (at the anodic and cathodic BPE edges) down to zero at the BPE center. This avoids a large increase in the required computational resources that would arise from calculating the floating potential of the BPE by an iterative numerical solution. Thus, the magnitude of the local faradaic current density was defined as:

$$j_{BPE}(x) = 2I_{BPE} \cdot \frac{abs\left(x - l_{elec}/2\right)}{l_{elec}/2} \tag{S13}$$

where I_{BPE} is the total electric current through the BPE and l_{elec} is the length of the BPE.

The above formal description was realized as a three-dimensional numerical scheme allowing us to resolve eqs 6-8 (main text), S1-S7, and S8-S13. This scheme was based on discrete three-dimensional spatiotemporal algorithms optimized for parallel computations. Particularly, the kinetic D_3Q_{19} lattice-Boltzmann equation method (LBM)[1] and the D_3Q_{19} lattice-based approaches developed by Warren[2] and by Capuani et al.[3] were employed to resolve numerically the electrohydrodynamic (eq 8, main text), electrostatic (eq 7, main text), and mass/charge

transport (eq 6, main text) problems, respectively. The D_3Q_{19} lattice is a projection of the four-dimensional face-centered hypercubic lattice onto three-dimensional space, where each lattice node is connected with 18 nearest and next-nearest neighbors. Such lattice connectivity is indispensable to achieve isotropic and Galilean-invariant transfer behavior of the modeled system. The body force was introduced into the LBM by the method of calculating the equilibrium distribution function with an altered velocity.[4]

As the modeled system exhibits a wide range of relaxation times (mainly due to very different characteristic times and lengths), a non-uniform spatiotemporal grid was employed for the computer simulations. In particular, the elementary time step was varied from 10^{-5} s down to 10^{-8} s in proximity to the BPE surface, whereas the elementary space step was varied between 1×10^{-6} and 5×10^{-8} m. All numerical schemes were realized as parallel codes in C language using the Message Passing Interface (MPI) standard. The developed computational model was implemented at a supercomputer (SGI Altix 4700) of the “Leibniz-Rechenzentrum der Bayerischen Akademie der Wissenschaften” (Garching, Germany). A typical simulation to analyze the temporal behavior of the system for 100 s required ~8 h at 128 processor cores and around 20 GB of system memory.

Table S1. Reaction rate constants.[5-8]

Reaction rate constant	Value
Eq S1, $k_{f,S1}$	1.0×10^{10} $M^{-1}s^{-1}$
Eq S1, $k_{b,S1}$	2.1×10^{2} $M^{-1}s^{-1}$
Eqs S2 and S7, $k_{f,S2}$	1.4×10^{-3} Ms^{-1}
Eqs S2 and S7, $k_{b,S2}$	1.4×10^{11} $M^{-1}s^{-1}$
Eq S3, $k_{f,S3}$	3.7×10^{-2} s^{-1}
Eq S3, $k_{b,S3}$	8.7×10^{3} $M^{-1}s^{-1}$
Eq S4, $k_{f,S4}$	1.2×10^{4} $M^{-1}s^{-1}$
Eq S4, $k_{b,S4}$	4.0×10^{4} $M^{-1}s^{-1}$
Eq S5, $k_{f,S5}$	5.0×10^{10} $M^{-1}s^{-1}$
Eq S5, $k_{b,S5}$	2.8 $M^{-1}s^{-1}$
Eq S6, $k_{f,S6}$	6.0×10^{9} $M^{-1}s^{-1}$
Eq S6, $k_{b,S6}$	1.1×10^{6} $M^{-1}s^{-1}$

Here, $k_{f,S1}$ and $k_{b,S1}$ denote the rate constants of the forward and backward reactions, respectively, presented by equation S1. The notation for the other rate constants follows this scheme.

Enrichment of $[Ru(bpy)_3]^{2+}$ for an extended time period. Figure S1 shows an experiment similar to that in Figure 3 (main text), except the initial $[Ru(bpy)_3]^{2+}$ concentration was 1.0 μM instead of 10.0 μM. Also, the enrichment was allowed to proceed for 20 min, 4 times longer than the experiments shown in the main text. These data demonstrate that, in the carbonate buffer, enrichment could be initiated with a lower initial concentration compared to the Tris system. They also show that the greater band stability in the carbonate system allows the enrichment to proceed for longer times than for the Tris system, resulting in greater enrichment factors, 274 in carbonate buffer vs. 141 in Tris.

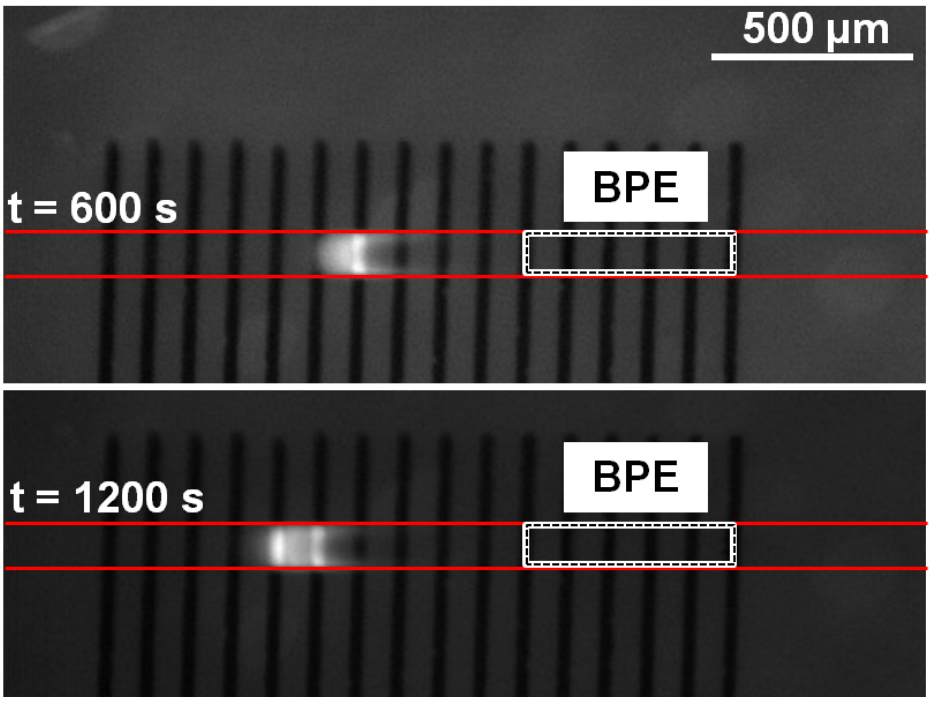

Figure S1. Fluorescence micrographs showing enrichment of $[Ru(bpy)_3]^{2+}$ by applying E_{tot} = 30.0 V to a 6 mm-long microchannel. The initial concentrations in the microchannel were 1.0 mM carbonate buffer (pH 10.0) and 1.0 μM $[Ru(bpy)_3]^{2+}$, and the BPE had a length of 500 μm. The enrichment factors were 160 (600 s), and 274 (1200 s).

References

1. Chen, S.; Doolen, G. D. *Annu. Rev. Fluid Mech.* **1998**, *30*, 329-364.
2. Warren, P. B. *Int. J. Mod. Phys. C* **1997**, *8*, 889-898.
3. Capuani, F.; Pagonabarraga, I.; Frenkel, D. *J. Chem. Phys.* **2004**, *121*, 973-986.
4. Shan, X. W.; Doolen, G. *J. Stat. Phys.* **1995**, *81*, 379-393.
5. Strehlow, H. *Techniques in Organic Chemistry*, ed. S.L. Friess, E.S. Lewis, and A. Weissberger. Vol. XIII. Wiley: New York, 1963.
6. Eigen, M. *Angew. Chem. Int. Ed.* **1964**, *3*, 1-19.
7. Johnson, K. S. *Limnol. Oceanogr.* **1982**, *27*, 849-855.
8. Wang, X. G.; Conway, W.; Burns, R.; McCann, N.; Maeder, M. *J. Phys. Chem. A* **2010**, *114*, 1734-1740.